PERGAMON

International Journal of Solids and Structures 39 (2002) 1515–1537

INTERNATIONAL JOURNAL OF SOLIDS and STRUCTURES

www.elsevier.com/locate/ijsolstr

Analysis of local delaminations in composite laminates with angle-ply matrix cracks

Maria Kashtalyan, Costas Soutis *

Department of Aeronautics, Imperial College of Science, Technology and Medicine, Prince Consort Road, London SW7 2BY, UK

Received 11 April 2001; received in revised form 8 November 2001

Abstract

In this paper, local delaminations growing uniformly from the tips of angle-ply matrix cracks in composite laminates loaded in tension are modelled theoretically. A 2-D shear lag method is used to determine stresses in a laminate representative segment containing one crack and two crack tip delaminations. For the calculation of the strain-energy release rate (SERR) associated with delaminations, the damaged layer is replaced with an equivalent homogeneous one with effective elastic properties. Closed-form expressions for the total SERR and its mode I and mode II components as a linear function of the first partial derivatives of the effective elastic properties of the damaged layer with respect to delamination area are derived. Dependence of SERRs and the laminate stiffness properties on delamination area, crack density and ply orientation angle is examined for balanced $[0_2/\theta_2/-\theta_2]_s$ and unbalanced $[0_2/\theta_2]_s$ carbon/epoxy laminates. The total SERR obtained in this study is compared to a simple closed-form expression for a uniform local delamination derived in earlier work by O'Brien (Local delamination in laminates with angle-ply matrix cracks: Part II Delamination Fracture Analysis and Fatigue Characterization. NASA Technical Memorandum 104076/AVSCOM Technical Report 91-B-011). It appears that matrix crack density and delamination size influence the SERR value significantly.

Keywords: Composite materials; Delamination; Fracture; Micromechanics; Modelling; Shear lag; Stiffness

1. Introduction

Delamination is a commonly observed failure mode in fibre-reinforced composite laminates subjected to static or fatigue tensile or thermal loading. Its initiation is often triggered by resin (matrix) cracks running parallel to the fibres in off-axis plies of the laminate, which result in high interlaminar stresses at the ply interface.

Studies of delaminations induced by matrix cracking have been focusing predominantly on delaminations caused by transverse cracks, i.e. matrix cracks in the 90° plies of a laminate. Crossman and Wang (1982) made comprehensive observations of transverse cracking and delamination in balanced symmetric $[\pm 25/90_n]_s$, $n = 0.5;1;2;3;4;6;8$ graphite/epoxy laminates. A significant reduction in the delamination onset

* Corresponding author. Tel.: +44-(0)20-7594-5070; fax: +44-(0)20-7584-8120.
E-mail addresses: m.kashtalyan@ic.ac.uk (M. Kashtalyan), c.soutis@ic.ac.uk (C. Soutis).

0020-7683/02/$ - see front matter
PII: S0020-7683(02)00007-0

strain was noted for the laminates with $n \geqslant 4$. A transition from edge delamination to local delaminations growing from the tip of a matrix crack in the 90° ply occurred between $n = 3$ and 4. O'Brien (1982) observed the onset and growth of edge delamination in $[(\pm 30)_2/90/\overline{90}]_s$ graphite/epoxy laminates under static tension and tension–tension fatigue loading. Stiffness loss was monitored simultaneously with delamination growth and found to decrease linearly with delamination size. Initiation and growth of local delaminations from the tips of transverse cracks in cross-ply $[0/90_n]_s$ $n = 2;4;6$ carbon/epoxy laminates under static tension was examined by Takeda and Ogihara (1994). Delamination was noted to grow more rapidly and extensively in the laminates with thicker 90° plies.

O'Brien (1985) suggested a simple closed-form expression for the strain-energy release rate (SERR) for local delaminations growing uniformly from transverse crack tips. The expression is based on simple load shearing rules and the classical laminated plate theory. It gives the SERR that depends only on the laminate lay-up and thickness, the location of the cracked ply and subsequent delaminations, the applied load and the laminate width, and is independent of delamination size. Also, the expression does not take into account the cumulative effect of damage.

Using a quasi-3D finite element (FE) analysis, Salpekar and O'Brien (1991) found that the SERR for uniform local delamination calculated from O'Brien (1985) expression matched the value obtained by FE analysis in the laminate interior. FE results for uniform local delaminations initiating from a transverse crack in cross-ply $[0_2/90_4]_s$ and balanced $[\pm 45/90_4]_s$ glass/epoxy laminates indicated that the SERR was higher near the free edge. It increased with delamination length and reached a constant value at delamination length of about four-ply thicknesses from the transverse crack in the interior as well as near the edges. However, the peak value of SERR near the free edge has yet to be verified by convergence studies (Bystrov, 2000).

Armanios et al. (1991) applied a shear deformation theory and sub-laminate approach to analyse local delaminations originating from transverse cracks in $[\pm 25/90_n]_s$ laminates. Predictions of their model, which also takes into account hygrothermal effects, are in reasonable agreement with delamination onset strain data by Crossman and Wang (1982).

Nairn and Hu (1992) conducted a two-dimensional variational analysis of crack-tip delaminations in $[(S)/90_n]_s$ laminates, where (S) denotes a balanced sub-laminate, e.g. $(\pm\theta_m)$. They predicted that matrix cracking should reach some critical density before delamination initiates. The critical crack density for delamination initiation is determined by material properties, laminate structure as well as fracture toughnesses for matrix cracking and delamination. It is nearly independent of the properties of the supporting sub-laminate (S).

More recently, Ashkantala and Talreja (1998) and Berthelot and Le Corre (2000) examined transverse crack-tips delaminations in cross-ply laminates with shear friction between the delaminated plies. While Berthelot and Le Corre (2000) assumed the magnitude of the interlaminar shear stress at the delaminated interface to be constant, i.e. independent of delamination length, Ashkantala and Talreja (1998) considered both linear and cubic polynomial shear stress distribution at the delamination interface.

Zhang et al. (1999) studied delaminations induced by transverse cracking at the $(\phi/90)$ interfaces in $[\ldots/\varphi_i/\phi_m/90_n]_s$ laminates loaded in tension. In particular, they were interested in the constraining effect of the immediate neighbouring plies and remote plies on stiffness reduction and SERR for delaminations. A sub-laminate-wise first-order shear deformation theory was used to analyse stress and strain fields. It was found that the SERR for local delamination and stiffness reduction of the constrained transverse plies largely depends on a local lay-up configuration of a damaged laminate. The authors suggested that SERR for local delamination at the $(\phi/90)$ interface in a $[\ldots/\varphi_i/\phi_m/90_n]_s$ can be analysed using a $[\phi_m/90_n]_s$ laminate, where the 90° plies and their next neighbouring plies are subjected to the same laminate strain.

The shear lag method was successfully used by several authors to model onset and growth of transverse crack-tip delaminations. Dharani and Tang (1990) used shear lag method to determine the interlaminar shear and normal stresses at the delamination tip. Delamination was assumed to occur when the maximum

interlaminar shear stress reached a critical value. Governing equations, formulated in terms of finite differences, were solved numerically using an eigen-value technique.

Zhang et al. (1994a,b) used a 2-D improved shear lag analysis to predict the SERR for edge and local delaminations in balanced symmetric $[\pm\theta_m/90_n]_s$ laminates. For edge delamination, they were able to capture a zigzag delamination pattern, i.e. edge delamination switching from one $(\theta/90)$ interface to another through a matrix crack, and improve O'Brien's formula for SERR for edge delamination (O'Brien, 1982) incorporating the effect of matrix cracking. For local delaminations, they obtained the SERR as a function of crack density and delamination area. Their predictions for delamination onset strain agree well with experimental data of Crossman and Wang (1982) and capture the transition from edge to local delamination quite accurately.

Ogihara and Takeda (1995) used a modified shear lag method featuring interlaminar shear layer to predict SERR and Young's modulus reduction due to transverse crack tip delaminations in cross-ply $[0/90_n]_s$ laminates and to model interaction between transverse cracking and delamination. However, the effect of cracking/delamination interaction was found to be negligible in prediction of delamination growth.

More recently, Selvarathinam and Weitsman (1999) observed and modelled, by means of shear lag method, delaminations induced by matrix cracking in cross-ply laminates under environmental fatigue. By comparing SERRs associated with matrix cracking and delamination, they were able to explain the extensive delaminations and reduced crack densities that arise under immersed fatigue conditions, as compared with fatigue in air.

Berthelot and Le Corre (2000) applied shear lag method to analyse the stress fields in cross-ply laminates containing transverse cracks and crack tip delaminations with shear friction between the delaminated plies.

Using an improved 2-D shear lag method (Zhang et al., 1994b) and Equivalent Constraint Model of the damaged ply (Fan and Zhang, 1993), Kashtalyan and Soutis (1999, 2000a) examined the effect of crack-tip delaminations on stiffness reduction. For cross-ply $[0_m/90_n]_s$ laminates, local delaminations along transverse as well as longitudinal cracks were considered. It was established that reduction in the laminate shear modulus and Poisson's ratio is much more significant than in the axial modulus. For balanced symmetric $[\pm\theta_m/90_n]_s$, the effect of constraining ply orientation angle θ on reduction of the laminate in-plane stiffness properties was also examined.

While transverse crack-tip delaminations have been the subject of numerous studies in the literature, delaminations growing from the tips of angle-ply cracks have received considerably less attention.

O'Brien and Hooper (1991) and O'Brien (1991) observed matrix-crack-induced delaminations in symmetric angle ply $[0_2/\theta_2/-\theta_2]_s$ carbon/epoxy laminates under quasi-static and fatigue tensile loading $(\theta = 15°; 20°; 25°; 30°)$. Delaminations occurred in the $(\theta/-\theta)$ interface, bounded by the cracks in the $(-\theta)$ ply and the stress-free edge. The laminated plate theory and a quasi-3D FE analysis were used to examine stresses in the $(-\theta)$ ply. For the considered range of ply orientations, stresses normal to the fibres were found to be compressive and shear stresses along the fibres to be high in the laminate interior, while near the free edge high tensile stresses normal to the fibres were present. Two closed-form expressions for SERR were derived on the basis of simple load shearing rules: one for a local delamination growing from an angle-ply matrix crack with a uniform delamination front across the laminate width (Fig. 1a), and one for a partial local delamination growing from an angle-ply matrix crack and bounded by the free edge (Fig. 1b). As for the transverse crack tip delamination (O'Brien, 1985), SERR for uniform local delamination was independent of delamination size and matrix crack density, while for partial local delamination it depended on delamination length. However, when the matrix crack length and the corresponding delamination length along the free edge is small, the difference between the uniform and partial delamination solutions was found to be insignificant.

Salpekar and O'Brien (1993) used a 3-D FE analysis to study matrix-crack-induced delaminations in $(0/\theta/-\theta)_s$ graphite/epoxy laminates $(\theta = 15°; 45°)$ loaded in tension. For $(0/45/-45)_s$ laminate, the SERR for local delamination growing uniformly in the $(45/-45)$ interface from the matrix crack in the $(-45°)$ ply was found to be higher near the laminate edge than in the interior of the laminate.

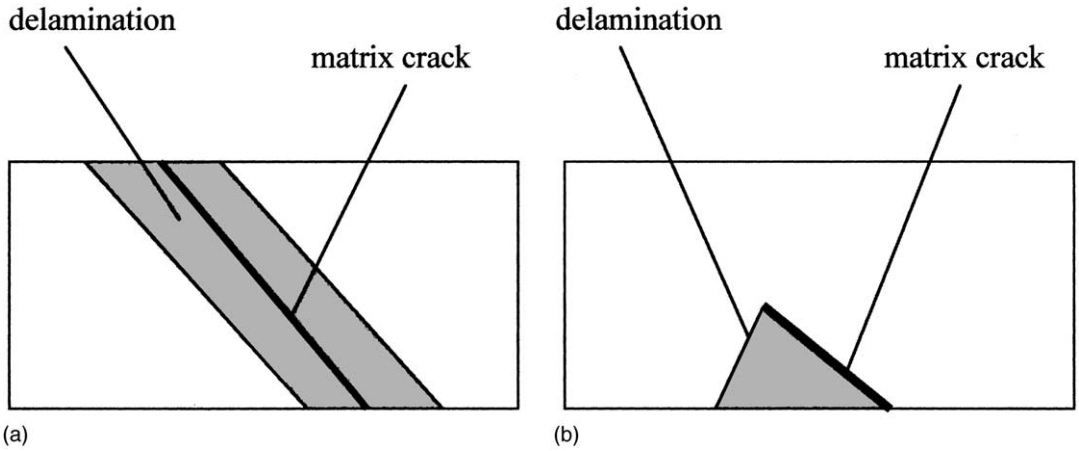

Fig. 1. Local delamination induced by angle-ply matrix cracks: (a) uniform across the laminate width; (b) partial.

Later, Salpekar et al. (1996) computed SERRs associated with local delamination originating from matrix cracks and bounded by the free edge in $(0/\theta/-\theta)_s$ and $(\theta/-\theta/0)_s$ graphite/epoxy laminates using a 3-D FE method. The total SERR was calculated using three different techniques: the virtual crack closure technique, the equivalent domain integral technique, and the global energy balance technique. For both lay-ups analysed, the fraction of the total SERR associated with mode I was greatest near the matrix crack and decreased near the free edge. It also decreased with increasing delamination length and was influenced by matrix crack length. However, no comparison with O'Brien's (1991) closed-form expressions for uniform and partial local delaminations was made.

In this paper, local delaminations growing uniformly from the tips of pre-existing matrix cracks in the mid-layer of a general symmetric laminate loaded in tension are modelled theoretically using the approach by Zhang et al. (1994b), initially developed for local delaminations growing from the transverse crack tips in balanced symmetric $[\pm\theta_m/90_n]_s$ laminates. Here, it is extended to local delaminations associated with angle-ply matrix cracks and used to predict SERR and the laminate residual stiffness as functions of matrix crack density and delamination length. For the SERR, comparison with the O'Brien's closed-form expression for uniform local delamination (O'Brien, 1991) is made. The issue of transition from angle-ply matrix cracking to delamination has not been addressed in the paper and is a subject of ongoing research. For transverse cracking in the 90° ply, energetic considerations governing transition to local delamination have been examined by Nairn and Hu (1992) and Selvarathinam and Weitsman (1998).

2. Stress analysis

A schematic of a symmetric $[(S)/\phi]_s$ laminate, consisting of the outer sub-laminate (S) and the inner ϕ layer damaged by matrix cracks and local delaminations growing from their tips at the $(S)/\phi$ interface is shown in Fig. 2. The outer sub-laminate (S), or layer 1, may consist either of a single layer or a group of layers and can also be damaged (in this case it needs to be replaced in the analysis with an equivalent homogeneous layer with reduced stiffness properties). The laminate is referred to the global Cartesian co-ordinate system xyz and local co-ordinate system $x_1x_2x_3$, with the axis x_1 directed along the fibres in the damaged ϕ layer, or layer 2. The laminate is subjected to in-plane biaxial tension $\bar{\sigma}_x$ and $\bar{\sigma}_y$. Since the laminate is symmetric, no coupling exists between in-plane loading and out-of-plane deformation. Matrix

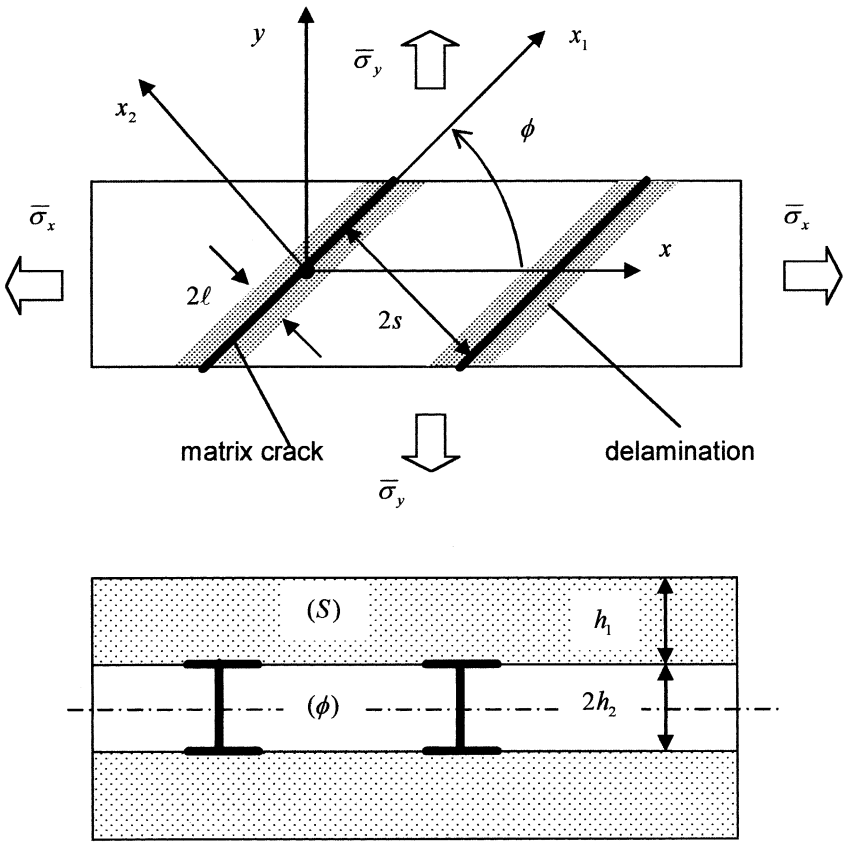

Fig. 2. Front and edge view of a $[(S)/\phi]_s$ laminate subjected to biaxial tensile loading and damaged by matrix cracks and uniform local delaminations. Local ($x_1x_2x_3$) and global (xyz) co-ordinate systems for the damaged ϕ layer (front view in the negative $x_3 \equiv z$ direction).

cracks are assumed to be spaced uniformly, with crack spacing $2s$ and span the whole width of the laminate. Local delaminations are assumed to be strip shaped, with strip width 2ℓ (Fig. 2).

Due to the periodicity of damage, the stress analysis may be carried out over a representative segment containing one matrix crack and two crack-tip delaminations. Due to symmetry, it can be further restricted to one quarter of the representative segment (Fig. 3), referred to the local co-ordinate system $x_1x_2x_3$.

Let $\{\tilde{\sigma}^{(1)}\}$ and $\{\tilde{\varepsilon}^{(1)}\}$ denote the in-plane microstresses and microstrains in the layer 1, and $\{\tilde{\sigma}^{(2)}\}$ and $\{\tilde{\varepsilon}^{(2)}\}$ denote the in-plane microstresses and microstrains in the layer 2 (i.e. stresses and strains averaged across the respective layer thickness). Since it is assumed that there is no frictional contact between the layers in the locally delaminated portion of the representative segment ($0 < |x_2| < \ell, |x_3| < h_2$), the in-plane microstresses in the delaminated portion are $\tilde{\sigma}_{22}^{(2)} = \tilde{\sigma}_{12}^{(2)} = 0$, i.e. this region is stress free. Assumption of stress-free crack tip delamination surfaces, and the resulting implication that the portion of the damaged ply bounded by matrix crack and delamination surfaces is stress free, has been widely used in the studies of delaminations. Besides that, delaminations were assumed to behave in a self-similar manner, i.e. the boundary conditions prescribed at the delaminated surfaces were assumed to be the same for small and large delaminations.

In the perfectly bonded region ($\ell < |x_2| < s$) of the representative segment, they are determined from the equilibrium equations

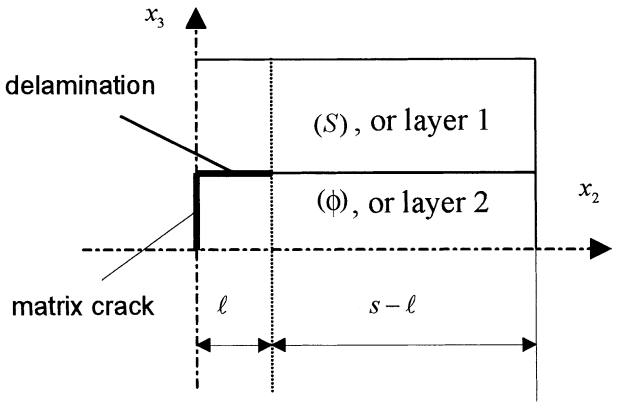

Fig. 3. A quarter of the representative segment containing a matrix crack and delamination.

$$\frac{\mathrm{d}}{\mathrm{d}x_2}\tilde{\sigma}_{j2}^{(2)} - \frac{\tau_j}{h_2} = 0, \quad j = 1,2 \tag{1}$$

where τ_j are the interface shear stresses and h_2 is the thickness of the ϕ layer.

By averaging the out-of-plane constitutive equations for both layers across the layer thickness, the interface shear stresses τ_j can be expressed in terms of the in-plane displacements and shear lag parameters K_{12}^{21} as

$$\tau_j = K_{j1}(\tilde{u}_1^{(1)} - \tilde{u}_1^{(2)}) + K_{j2}(\tilde{u}_2^{(1)} - \tilde{u}_2^{(2)}) \tag{2}$$

The shear lag parameters K_{11}, K_{22}, $K_{12} \equiv K_{21}$ are determined assuming that the out-of-plane shear stresses $\tilde{\sigma}_{j3}^{(k)}$ vary linearly with x_3 (Fig. 4), see Appendix A. Substitution of Eq. (2) into Eq. (1) and subsequent differentiation yields

$$\frac{\mathrm{d}^2}{\mathrm{d}x_2}\tilde{\sigma}_{j2}^{(2)} + K_{j1}(\tilde{\gamma}_{12}^{(1)} - \tilde{\gamma}_{12}^{(2)}) + K_{j2}(\tilde{\varepsilon}_{22}^{(1)} - \tilde{\varepsilon}_{22}^{(2)}) = 0, \quad j = 1,2 \tag{3}$$

The strain differences $(\tilde{\varepsilon}_{22}^{(1)} - \tilde{\varepsilon}_{22}^{(2)})$ and $(\tilde{\gamma}_{12}^{(1)} - \tilde{\gamma}_{12}^{(2)})$, involved in Eq. (3), can be expressed in terms of stresses $\tilde{\sigma}_{12}^{(2)}$, $\tilde{\sigma}_{22}^{(2)}$ using the constitutive equations for both layers, the laminate equilibrium equations below

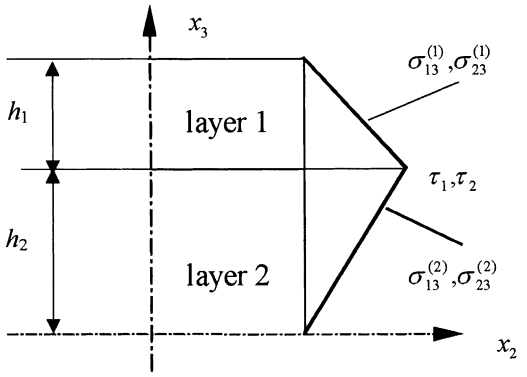

Fig. 4. Variation of out-of-plane shear stresses.

$$\chi\{\tilde{\sigma}^{(1)}\} + \{\tilde{\sigma}^{(2)}\} = (1+\chi)[T]\{\bar{\sigma}\} \tag{4a}$$

$$[T] = \begin{bmatrix} \cos^2\phi & \sin^2\phi & 2\sin\phi\cos\phi \\ \sin^2\phi & \cos^2\phi & -2\sin\phi\cos\phi \\ -\sin\phi\cos\phi & \sin\phi\cos\phi & \cos^2\phi - \sin^2\phi \end{bmatrix} \tag{4b}$$

$$\{\bar{\sigma}\} = \{\sigma_x, \sigma_y, 0\}^{\mathrm{T}}, \qquad \chi = h_1/h_2 \tag{4c}$$

and the assumption of the generalised plane strain condition

$$\tilde{\varepsilon}_{11}^{(1)} = \tilde{\varepsilon}_{11}^{(2)} \tag{5}$$

In the local co-ordinate system $x_1x_2x_3$, the layer 2 is orthotropic,

$$\begin{Bmatrix} \tilde{\varepsilon}_{11}^{(2)} \\ \tilde{\varepsilon}_{22}^{(2)} \\ \tilde{\gamma}_{12}^{(2)} \end{Bmatrix} = \begin{bmatrix} \widehat{S}_{11}^{(2)} & \widehat{S}_{12}^{(2)} & 0 \\ \widehat{S}_{12}^{(2)} & \widehat{S}_{22}^{(2)} & 0 \\ 0 & 0 & \widehat{S}_{66}^{(2)} \end{bmatrix} \begin{Bmatrix} \tilde{\sigma}_{11}^{(2)} \\ \tilde{\sigma}_{22}^{(2)} \\ \tilde{\sigma}_{12}^{(2)} \end{Bmatrix} \tag{6a}$$

while the layer 1 is anisotropic

$$\begin{Bmatrix} \tilde{\varepsilon}_{11}^{(1)} \\ \tilde{\varepsilon}_{22}^{(1)} \\ \tilde{\gamma}_{12}^{(1)} \end{Bmatrix} = \begin{bmatrix} \widehat{S}_{11}^{(1)} & \widehat{S}_{12}^{(1)} & \widehat{S}_{16}^{(1)} \\ \widehat{S}_{12}^{(1)} & \widehat{S}_{22}^{(1)} & \widehat{S}_{26}^{(1)} \\ \widehat{S}_{16}^{(1)} & \widehat{S}_{26}^{(1)} & \widehat{S}_{66}^{(1)} \end{bmatrix} \begin{Bmatrix} \tilde{\sigma}_{11}^{(1)} \\ \tilde{\sigma}_{22}^{(1)} \\ \tilde{\sigma}_{12}^{(1)} \end{Bmatrix} \tag{6b}$$

where $[\widehat{S}^{(k)}]$ is the compliances matrix for the kth layer.

Finally, Eq. (3) can be reduced to a system of two coupled second order ordinary differential equations (see Appendix B)

$$\frac{\mathrm{d}^2\tilde{\sigma}_{12}^{(2)}}{\mathrm{d}x_2^2} - N_{11}\tilde{\sigma}_{12}^{(2)} - N_{12}\tilde{\sigma}_{22}^{(2)} - P_{11}\bar{\sigma}_x - P_{12}\bar{\sigma}_y = 0 \tag{7a}$$

$$\frac{\mathrm{d}^2\tilde{\sigma}_{22}^{(2)}}{\mathrm{d}x_2^2} - N_{21}\tilde{\sigma}_{12}^{(2)} - N_{22}\tilde{\sigma}_{22}^{(2)} - P_{21}\bar{\sigma}_x - P_{22}\bar{\sigma}_y = 0 \tag{7b}$$

Here N_{ij} and P_{ij} are laminate constants depending on the layer compliances $\widehat{S}_{ij}^{(k)}$, layer thickness ratio χ, shear lag parameters K_{11}, K_{22}, K_{12} and angle ϕ (see Appendix B). Eqs. (7a) and (7b) can be uncoupled at the expense of increasing the order of differentiation, resulting in a fourth order non-homogeneous ordinary differential equation

$$\frac{\mathrm{d}^4\tilde{\sigma}_{22}^{(2)}}{\mathrm{d}x_2^4} - (N_{11}+N_{22})\frac{\mathrm{d}^2\tilde{\sigma}_{22}^{(2)}}{\mathrm{d}x_2^2} - (N_{21}N_{12} - N_{11}N_{22})\tilde{\sigma}_{22}^{(2)} + [N_{11}(P_{21}+\alpha P_{22}) - N_{21}(P_{11}+\alpha P_{12})]\bar{\sigma}_x = 0 \tag{8}$$

Here $\alpha = \bar{\sigma}_y/\bar{\sigma}_x$ is the biaxiality ratio. The boundary conditions for Eq. (8) are prescribed at the stress-free boundary between locally delaminated and perfectly bonded portions of the representative segment

$$\tilde{\sigma}_{22}^{(2)}|_{x_2=\pm\ell} = 0 \qquad \tilde{\sigma}_{12}^{(2)}|_{x_2=\pm\ell} = 0 \tag{9}$$

Finally, the in-plane microstresses can be expressed in the following form

$$\tilde{\sigma}_{11}^{(2)} = a_{22}\tilde{\sigma}_{22}^{(2)} + a_{12}\tilde{\sigma}_{12}^{(2)} + b_x\bar{\sigma}_x + b_y\bar{\sigma}_y \tag{10a}$$

$$\tilde{\sigma}_{j2}^{(2)} = \left[A_j \frac{\cosh \lambda_1 (x_2 - s)}{\cosh \lambda_1 (s - \ell)} + B_j \frac{\cosh \lambda_2 (x_2 - s)}{\cosh \lambda_2 (s - \ell)} + C_j \right] \bar{\sigma}_x, \quad j = 1, 2 \tag{10b}$$

where coefficients a_{22}, a_{12}, b_x and b_y are given in Appendix B, λ_j are the roots of the characteristic equation and A_j, B_j and C_j are constants depending on N_{ij} and P_{ij}, see Appendix C.

The in-plane microstresses are required to estimate the stiffness matrix of the damaged layer and subsequently the residual stiffness properties of the entire laminate, as described in the following section.

3. Stiffness reduction

To determine the reduced stiffness properties of the damaged laminate, an equivalent laminate, in which the damaged layer is replaced with an equivalent homogeneous one with degraded stiffness properties, is considered. In the local co-ordinate system $x_1x_2x_3$, the constitutive equations of the equivalent homogeneous layer are

$$\{\bar{\sigma}^{(2)}\} = [Q^{(2)}]\{\bar{\varepsilon}^{(2)}\} \tag{11}$$

In the local co-ordinates, the modified in-plane stiffness matrix $[Q^{(2)}]$ of the homogeneous layer equivalent to the damaged one is related to the in-plane stiffness matrix $[\widehat{Q}^{(2)}]$ of the undamaged layer as

$$[Q^{(2)}] = [\widehat{Q}^{(2)}] - \begin{bmatrix} (\widehat{Q}_{12}^{(2)})^2 / \widehat{Q}_{22}^{(2)} \Lambda_{22} & \widehat{Q}_{12}^{(2)} \Lambda_{22} & 0 \\ \widehat{Q}_{12}^{(2)} \Lambda_{22} & \widehat{Q}_{22}^{(2)} \Lambda_{22} & 0 \\ 0 & 0 & \widehat{Q}_{66}^{(2)} \Lambda_{66} \end{bmatrix} \tag{12}$$

Here Λ_{22}, Λ_{66} are the in-situ damage effective functions (IDEFs) (Zhang et al., 1994b). They can be expressed in terms of lamina macrostresses and macrostrains as

$$\Lambda_{22} = 1 - \frac{\bar{\sigma}_{22}^{(2)}}{\widehat{Q}_{12}^{(2)} \bar{\varepsilon}_{11}^{(2)} + \widehat{Q}_{22}^{(2)} \bar{\varepsilon}_{22}^{(2)}}, \qquad \Lambda_{66} = 1 - \frac{\bar{\sigma}_{12}^{(2)}}{\widehat{Q}_{66}^{(2)} \bar{\gamma}_{12}^{(2)}} \tag{13}$$

The lamina macrostresses $\{\bar{\sigma}^{(2)}\}$ and macrostrains $\{\bar{\varepsilon}^{(2)}\}$ are obtained by averaging respectively microstresses $\{\tilde{\sigma}^{(2)}\}$ (Eqs. (10a) and (10b)) and microstrains $\{\tilde{\varepsilon}^{(2)}\}$ (Eq. (6a)), across the length of the representative segment. The lamina macrostresses $\bar{\sigma}_{ij}^{(2)}$ are

$$\bar{\sigma}_{11}^{(2)} = a_{22} \bar{\sigma}_{22}^{(2)} + a_{12} \bar{\sigma}_{12}^{(2)} + b_x \bar{\sigma}_x + b_y \bar{\sigma}_y, \qquad \lambda_j^* = h_2 \lambda_j \tag{14a}$$

$$\bar{\sigma}_{j2}^{(2)} = \left[A_j \frac{D^{mc}}{\lambda_1^* (1 - D^{ld})} \tanh \frac{\lambda_1^* (1 - D^{ld})}{D^{mc}} + B_j \frac{D^{mc}}{\lambda_2^* (1 - D^{ld})} \tanh \frac{\lambda_2^* (1 - D^{ld})}{D^{mc}} + C_j (1 - D^{ld}) \right] \bar{\sigma}_x, \quad j = 1, 2 \tag{14b}$$

where $D^{mc} = h_2/s$ denotes relative crack density and $D^{ld} = \ell/s$ denotes relative delamination area. The macrostrains in the individual homogeneous layers and the laminate are assumed to be equal

$$\bar{\varepsilon}_{11}^{(1)} = \bar{\varepsilon}_{11}^{(2)} = \bar{\varepsilon}_{11}, \qquad \bar{\varepsilon}_{22}^{(1)} = \bar{\varepsilon}_{22}^{(2)} = \bar{\varepsilon}_{22}, \qquad \bar{\gamma}_{12}^{(1)} = \bar{\gamma}_{12}^{(2)} = \bar{\gamma}_{12} \tag{15}$$

Using the constitutive equations for the layer 1 (Eq. (6b)) and equations of the global equilibrium of the laminate (Eq. (4a)–(4c)) the lamina macrostrains in the layer 2 are

$$\{\bar{\varepsilon}^{(2)}\} = [\widehat{S}^{(1)}] \chi^{-1} ((1 + \chi)[T]\{\bar{\sigma}\} - \{\bar{\sigma}^{(2)}\}) \tag{16}$$

where the transformation matrix $[T]$ is given by Eq. (4b). Thus, the lamina macrostresses (Eqs. (14a) and (14b)) and macrostrains (Eq. (16)) are determined as explicit functions of the damage parameters D^{mc}, D^{ld}.

Finally, the modified stiffness matrix $[\overline{Q}]_2$ of the equivalent homogeneous layer in the global co-ordinates xyz can be obtained from the modified stiffness matrix $[Q^{(2)}]$ in the local co-ordinates, Eq. (12) as

$$[\overline{Q}]_2 = [T]^{-1}[Q^{(2)}][T]^{-\mathrm{T}} \tag{17}$$

where the transformation matrix $[T]$ is given by Eq. (4b). The extension stiffness matrix $[\overline{A}]$ of the equivalent laminate in the global co-ordinates xyz can be calculated as

$$[\overline{A}] = \sum_k [\overline{Q}]_k h_k, \quad k = 1, 2 \tag{18}$$

where $[\overline{Q}]_1$ is the in-plane stiffness matrix of layer 1, or the outer sub-laminate, in the global co-ordinates.

4. Strain-energy release rate

The total SERR G^{ld} associated with local delaminations growing from the tips of matrix cracks is equal to the first partial derivative of the total strain energy U stored in the damaged laminate with respect to the total delamination area A^{ld} provided the applied strains $\{\bar{\varepsilon}\}$ are fixed and the matrix crack density $C = (2s)^{-1}$ remains unchanged

$$G^{ld} = -\left.\frac{\partial U}{\partial A^{ld}}\right|_{\{\bar{\varepsilon}\},C} \tag{19}$$

The SERR can be effectively calculated using the equivalent laminate introduced in the previous section. In the global co-ordinates, if hygrothermal effects are neglected, the total strain energy stored in the laminate element with a finite gauge length L and width w is

$$U = \frac{wL}{2}\{\bar{\varepsilon}\}^{\mathrm{T}}[\overline{A}]\{\bar{\varepsilon}\} \tag{20}$$

where the residual extension stiffness matrix $[\overline{A}]$ of the equivalent laminate is given by Eq. (18). Noting that the area of a single crack-tip delamination is $a^{ld} = 2\ell w/|\sin\phi|$, (Fig. 2), the total delamination area is equal to

$$A^{ld} = 2a^{ld}CL = 2LwD^{ld}/|\sin\phi| \tag{21}$$

Then the SERR, calculated from Eqs. (18)–(21) is

$$G^{ld}(\bar{\varepsilon}, D^{mc}, D^{ld}) = -\frac{h_2}{2}\{\bar{\varepsilon}\}^{\mathrm{T}}\frac{\partial[\overline{Q}]_2}{\partial D^{ld}}\{\bar{\varepsilon}\}|\sin\phi| \tag{22}$$

Under uniaxial strain, Eq. (22) simplifies to

$$G^{ld}(\bar{\varepsilon}_{xx}, D^{mc}, D^{ld}) = -\frac{h_2}{2}\bar{\varepsilon}_{xx}^2\frac{\partial\overline{Q}_{xx,2}}{\partial D^{ld}}|\sin\phi| \tag{23}$$

Calculation of the residual in-plane axial stiffness $\overline{Q}_{xx,2}$ using Eq. (12) and the transformation formulae given by Eq. (17), yields the SERR associated with local delamination in terms of the IDEFs Λ_{22}, Λ_{66} and stiffness properties of the undamaged material $\widehat{Q}_{ij}^{(2)}$ as

$$G^{ld}(\bar{\varepsilon}_{xx}, D^{mc}, D^{ld}) = \frac{h_2}{2}\bar{\varepsilon}_{xx}^2\left[\left(\frac{\widehat{Q}_{12}^{(2)2}}{\widehat{Q}_{22}^{(2)}}\cos^4\phi + 2\widehat{Q}_{12}^{(2)}\sin^2\phi\cos^2\phi + \widehat{Q}_{22}^{(2)}\sin^4\phi\right)\frac{\partial\Lambda_{22}}{\partial D^{ld}} + 4\widehat{Q}_{66}^{(2)}\sin^2\phi\cos^2\phi\frac{\partial\Lambda_{66}}{\partial D^{ld}}\right]|\sin\phi| \tag{24}$$

The first partial derivatives of IDEFs that appear in Eq. (24) are explicit functions of the damage parameters D^{mc}, D^{ld} and can be calculated analytically.

O'Brien (1991) suggested a simple closed-form expression for the total SERR associated with uniform local crack-tip delamination at the $(\theta/-\theta)$ interface in a $[0_2/\theta_2/-\theta_2]_s$ laminate with matrix cracks present in the $(-\theta)$ ply. In the nomenclature of this paper it is given by

$$\frac{G^{ld}}{\bar{\varepsilon}_{xx}^2} = \frac{3\widehat{E}_x^2 h}{2}\left(\frac{1}{4\widehat{E}_{ld}} - \frac{1}{6\widehat{E}_x}\right) \tag{25}$$

where h is the laminate thickness, $\widehat{E}_x$ and $\widehat{E}_{ld}$ are respectively the laminate modulus and the modulus of the locally delaminated sub-laminate as calculated from the laminated plate theory. Since the locally delaminated $[0_2/\theta_2]_T$ sub-laminate is asymmetric, the value of $\widehat{E}_{ld}$ in Eq. (25) will depend on whether the presence of bending-extension and shear-extension coupling is reflected in the modulus calculation. For all ply orientation angles θ (i.e. from 5° to 90°), the influence of shear-extension coupling on the value of $\widehat{E}_{ld}$ and therefore the SERR was found to be significant. The shear constraint resulted in a greater $\widehat{E}_{ld}$ and, hence, correspondingly lower SERR. However, the effect of bending-extension coupling was proved to be small (O'Brien, 1991). It is worth noticing that the SERR given by Eq. (25) is independent from the delamination size. Also, the effect of matrix cracking is not taken into account when calculating the laminate modulus $\widehat{E}_x$. It will be shown later that G^{ld} is reduced with increasing crack density.

It should be mentioned here that even under the uniaxial loading damage development in the off-axis plies of general symmetric laminates always occurs under mixed mode conditions due to shear-extension coupling. It is therefore important in the calculation of the total SERR to be able to separate mode I and mode II contributions. For a $[(S)/\phi]_s$ laminate with damaged ϕ layer modelled by an equivalent laminate, the total SERR for crack tip uniform local delaminations is equal to the first partial derivative of the portion of the total strain energy stored in the equivalent homogeneous layer with respect to damage area

$$G^{ld} = -\left.\frac{\partial U^{(2)}}{\partial A^{ld}}\right|_{\{\bar{\varepsilon}\},C} \tag{26}$$

In the local co-ordinates (Fig. 2), this portion of the total strain energy can be separated into extensional and shear parts

$$U^{(2)} = U_{\mathrm{I}}^{(2)} + U_{\mathrm{II}}^{(2)} = Lwh_2(\bar{\sigma}_{11}^{(2)}\bar{\varepsilon}_{11}^{(2)} + \bar{\sigma}_{22}^{(2)}\bar{\varepsilon}_{22}^{(2)}) + Lwh_2\bar{\sigma}_{12}^{(2)}\bar{\gamma}_{12}^{(2)} \tag{27}$$

Under uniaxial strain $\bar{\varepsilon}_{xx}$, strains and stresses in the equivalent homogeneous layer are

$$\{\bar{\varepsilon}^{(2)}\} = \{\cos^2\phi, \sin^2\phi, 2\cos\phi\sin\phi\}^{\mathrm{T}}\bar{\varepsilon}_{xx}, \qquad \{\bar{\sigma}^{(2)}\} = [Q^{(2)}]\{\cos^2\phi, \sin^2\phi, 2\cos\phi\sin\phi\}^{\mathrm{T}}\bar{\varepsilon}_{xx} \tag{28}$$

where the modified stiffness matrix $[Q^{(2)}]$ of the equivalent homogeneous layer in the local co-ordinates is given by Eq. (12). Substitution of Eqs. (21), (27) and (28) into Eq. (26) gives mode I and mode II contributions into the total SERR as follows:

$$G_{\mathrm{I}}^{ld} = -\frac{\partial U_{\mathrm{I}}^{(2)}}{\partial A^{ld}} = \frac{\bar{\varepsilon}_{xx}^2 h_2}{2}\left(\frac{\widehat{Q}_{12}^{(2)2}}{\widehat{Q}_{22}^{(2)}}\cos^4\phi + 2\widehat{Q}_{12}^{(2)}\sin^2\phi\cos^2\phi + \widehat{Q}_{22}^{(2)}\sin^4\phi\right)\frac{\partial\Lambda_{22}}{\partial D^{ld}}|\sin\phi| \tag{29}$$

$$G_{\mathrm{II}}^{ld} = -\frac{\partial U_{II}^{(2)}}{\partial A^{ld}} = 2\bar{\varepsilon}_{xx}^{2} h_2 \widehat{Q}_{66}^{(2)} \frac{\partial \Lambda_{66}}{\partial D^{ld}} \cos^2\phi |\sin^3\phi| \tag{30}$$

The resulting total SERR $G^{ld} = G_{\mathrm{I}}^{ld} + G_{\mathrm{II}}^{ld}$ coincides with Eq. (24).

5. Results and discussion

Uniform local delaminations induced by angle-ply matrix cracking both in balanced and unbalanced symmetric laminates will be analysed in this section. Matrix cracking in off-axis plies is known to introduce some shear-extension coupling into balanced symmetric angle-ply laminates (Soutis and Kashtalyan, 2000), however of much smaller extent than that exhibited in unbalanced symmetric angle-ply laminates. The lay-ups to represent balanced and unbalanced laminates were chosen respectively as $[0_2/\theta_2/-\theta_2]_s$ and $[0_2/\theta_2]_s$. The orientation of the cracked mid-layer layer is therefore $\phi = -\theta$ for $[0_2/\theta_2/-\theta_2]_s$ laminate and $\phi = \theta$ for $[0_2/\theta_2]_s$ laminate. The material system is AS4/3506-1 graphite/epoxy that was earlier considered by O'Brien and Hooper (1991) and O'Brien (1991). Its lamina properties are as follows: $E_{11} = 135$ GPa, $E_{22} = 11$ GPa, $G_{12} = 5.8$ GPa, $v_{12} = 0.301$, single ply thickness $t = 0.124$ mm.

5.1. Stress analysis

Balanced laminates: Fig. 5 shows the in-plane stresses in the $(-\theta)$ ply of the $[0_2/\theta_2/-\theta_2]_s$ laminate as function of ply orientation angle θ under uniaxial ($\bar{\sigma}_y/\bar{\sigma}_x = 0$) and biaxial ($\bar{\sigma}_y/\bar{\sigma}_x = 0.5; 1; 2$) tensile loading as calculated from the laminated plate theory (Daniel and Ishai, 1994). The applied stress is $\bar{\sigma}_x = 200$ MPa. The in-plane stresses were transformed into the local co-ordinate system (Fig. 2), in order to determine stresses normal to the fibres ($\tilde{\sigma}_{22}$) and shear stresses along the fibres ($\tilde{\sigma}_{12}$) since these stresses contribute directly to the formation of matrix cracks. Under uniaxial tension, stresses normal to the fibres in the $(-\theta)$ ply of the $[0_2/\theta_2/-\theta_2]_s$ laminate are compressive for $15° < \theta < 40°$ and tensile for $\theta > 40°$ (Fig. 5a).

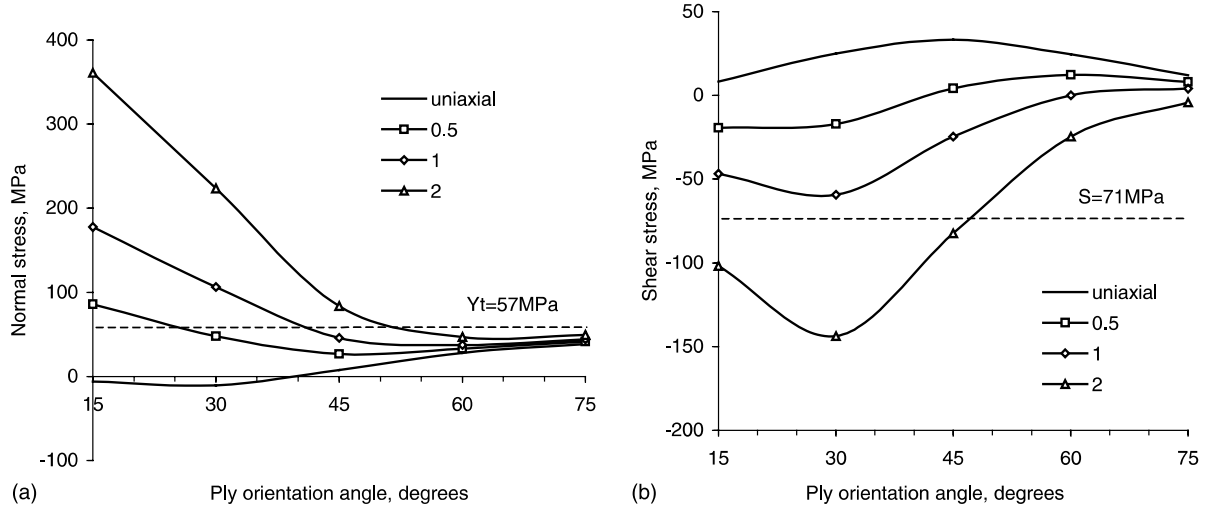

Fig. 5. Ply stresses in the $(-\theta)$ ply of a balanced symmetric $[0_2/\theta_2/-\theta_2]_s$ AS4/3506-1 laminate as function of ply orientation angle θ under uniaxial ($\bar{\sigma}_y/\bar{\sigma}_x = 0$) and biaxial ($\bar{\sigma}_y/\bar{\sigma}_x = 0.5; 1; 2$) tensile loading: (a) stresses normal to the fibres; (b) shear stresses. Applied stress $\bar{\sigma}_x = 200$ MPa.

However, a quasi-3D FE analysis by O'Brien and Hooper (1991) revealed that near the free edge, these stresses become tensile. This explains why, under uniaxial loading, matrix cracks in $[0_2/\theta_2/-\theta_2]_s$ laminates with $15^\circ \leqslant \theta \leqslant 30^\circ$ initiate at the free edge, but do not propagate into the laminate interior. Under biaxial loading, stresses in the $(-\theta)$ ply normal to the fibres are tensile. For all considered biaxiality ratios $\alpha = \bar{\sigma}_y/\bar{\sigma}_x$, the highest normal stresses are observed for $\theta = 15^\circ$. They decrease significantly as θ increases and at $\theta = 60^\circ$ reach almost a constant value that is almost independent of the biaxiality ratio. For $15^\circ \leqslant \theta \leqslant 60^\circ$, the magnitude of normal stresses increases with increasing biaxiality ratio, sometimes exceeding the value of the transverse tensile strength of the material. Under uniaxial tension, relatively high shear stresses are present along the fibres in the $(-\theta)$ ply of the $[0_2/\theta_2/-\theta_2]_s$ laminate (Fig. 5b).

In Fig. 5a and b the dotted line corresponds to the ultimate transverse tensile strength Y_t and shear strength S, respectively. According to the maximum stress criterion, once this value is exceeded, matrix cracking will occur. In the cracked configuration, the stresses in the damaged ply are defined by Eqs. (14a) and (14b) obtained from a 2-D shear lag analysis described earlier.

Unbalanced laminates: Fig. 6 shows the in-plane stresses in the θ ply of the $[0_2/\theta_2]_s$ laminate as function of ply orientation angle θ under uniaxial ($\bar{\sigma}_y/\bar{\sigma}_x = 0$) and biaxial ($\bar{\sigma}_y/\bar{\sigma}_x = 0.5; 1; 2$) tensile loading as calculated from the laminated plate theory (Daniel and Ishai, 1994). The applied stress is $\bar{\sigma}_x = 100$ MPa. Again, the in-plane stresses were transformed into the local co-ordinate system (Fig. 2) in order to determine stresses normal to the fibres ($\tilde{\sigma}_{22}$) and shear stresses along the fibres ($\tilde{\sigma}_{12}$) since these stresses contribute directly to the formation of matrix cracks. Under uniaxial tension, stresses normal to the fibres in the θ ply of the $[0_2/\theta_2]_s$ laminate are compressive for θ smaller than 25° and tensile for θ greater than 25° (Fig. 6a). Under biaxial loading, stresses in the (θ) ply normal to the fibres are tensile. For all considered biaxiality ratios $\alpha = \bar{\sigma}_y/\bar{\sigma}_x$, the highest normal stresses are observed for $\theta = 15^\circ$. They decrease significantly as θ increases and at $\theta = 75^\circ$ reach almost a constant value that is almost independent of the biaxiality ratio. For $15^\circ \leqslant \theta \leqslant 60^\circ$, the magnitude of normal stresses increases with increasing biaxiality ratio, sometimes exceeding the value of the transverse tensile strength of the material. Relatively low shear stresses are present along the fibres (Fig. 6b) in the θ ply of the $[0_2/\theta_2]_s$ laminate.

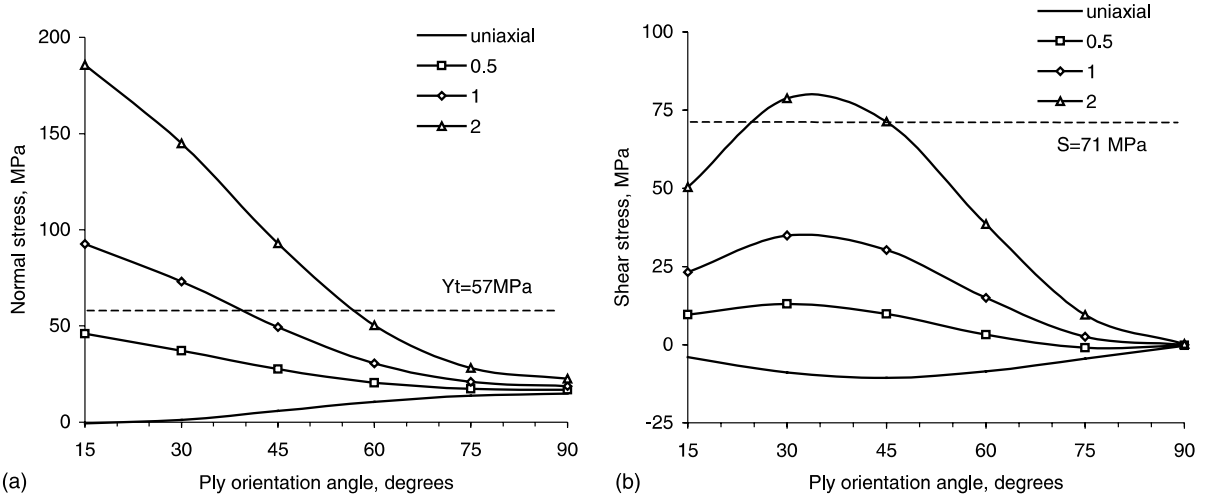

Fig. 6. Ply stresses in the (θ) ply of an unbalanced symmetric $[0_2/\theta_2]_s$ AS4/3506-1 laminate as function of ply orientation angle θ under uniaxial ($\bar{\sigma}_y/\bar{\sigma}_x = 0$) and biaxial ($\bar{\sigma}_y/\bar{\sigma}_x = 0.5; 1; 2$) tensile loading: (a) stresses normal to the fibres; (b) shear stresses. Applied stress $\bar{\sigma}_x = 100$ MPa.

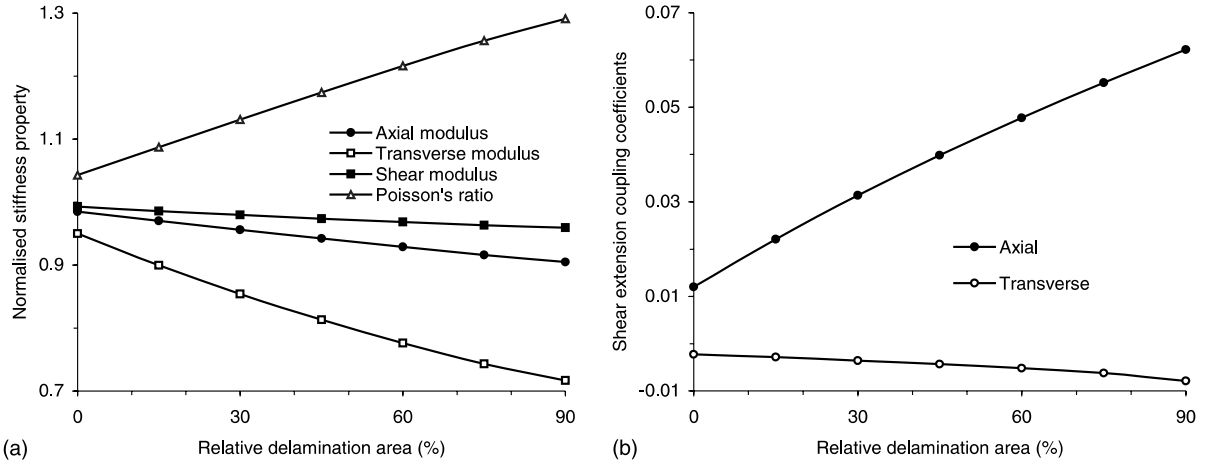

Fig. 7. Residual stiffness properties of a balanced symmetric $[0_2/30_2/-30_2]_s$ AS4/3506-1 laminate as a function of relative delamination area D^{ld}: (a) normalised moduli and Poisson's ratio; (b) shear-extension coupling coefficients. Matrix crack density 2 cracks/cm.

5.2. Stiffness degradation

Balanced laminates: Fig. 7 shows the variation of the laminate residual stiffness properties with the relative delamination area $D^{ld} = \ell/s$ in the $[0_2/30_2/-30_2]_s$ laminate. Axial modulus E_x, transverse modulus E_y, shear modulus G_{xy} and major Poisson's ratio v_{xy} normalised by their value for the undamaged laminate are plotted in Fig. 7a. The axial/transverse shear-extension coupling coefficients that characterise shearing in the xy plane caused by respectively axial/transverse stress are plotted in Fig. 7b. Matrix crack density in the inner $(-30°)$ ply is assumed equal to $C = 2$ cracks/cm. Values at $D^{ld} = 0$ indicate residual stiffness properties of the laminate at this crack density without delaminations. It can be seen that local delaminations further decrease the laminate moduli and, for the considered lay up, increase the Poisson's ratio (Fig. 7a). Matrix cracking in angle-ply laminates is known to introduce the coupling between extension and shear (Kashtalyan and Soutis, 2000b). In balanced $[0_2/\theta_2/-\theta_2]_s$ laminates uniform local delaminations result in an increase in the absolute value of the axial shear-extension coupling coefficient for $\theta < 45°$ and of the transverse shear-extension coupling coefficient for $\theta > 45°$. However, all shear-extension coupling coefficients are significantly smaller than those for unbalanced laminates (see later Fig. 8b).

Unbalanced laminates: Fig. 8 shows the variation of the laminate residual stiffness properties with the relative delamination area D^{ld} in the $[0_2/30_2]_s$ laminate. Axial modulus E_x, transverse modulus E_y, shear modulus G_{xy} and major Poisson's ratio v_{xy} normalised by their value for the undamaged laminates are plotted in Fig. 8a. The axial/transverse shear-extension coupling coefficients that characterise shearing in the xy plane caused by respectively axial/transverse stress are plotted in Fig. 8b. Matrix crack density in the 30° ply is assumed equal to $C = 2$ cracks/cm, values at $D^{ld} = 0$ indicate residual stiffness properties of the laminates at this crack density without delaminations. It can be seen that reduction of the laminate moduli and, for the considered lay up, increase the Poisson's ratio due to local delaminations are more significant in the unbalanced $[0_2/30_2]_s$ laminate than in the balanced $[0_2/30_2/-30_2]_s$ laminate with the same orientation of the damaged ply. Matrix cracking and crack tip delaminations are expected to amplify the shear-extension coupling exhibited in the undamaged unbalanced $[0_2/\theta_2]_s$ laminates. As in balanced $[0_2/\theta_2/-\theta_2]_s$ laminates, crack tip uniform local delaminations in unbalanced laminates result in an increase in the absolute value of the axial shear-extension coupling coefficient for $\theta < 45°$ and of the transverse shear-extension coupling coefficient for $\theta > 45°$.

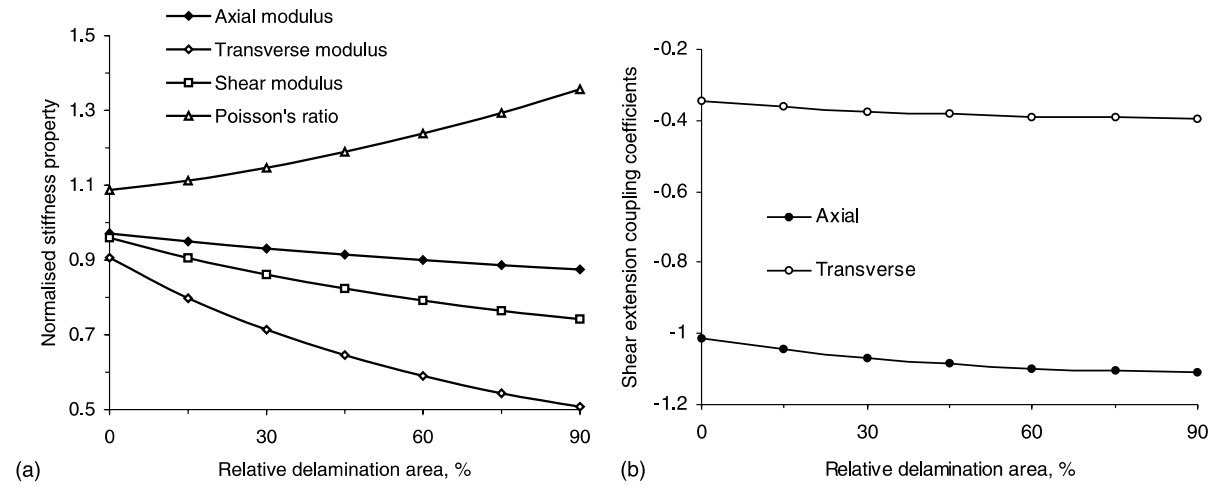

Fig. 8. Residual stiffness properties of an unbalanced symmetric $[0_2/30_2]_s$ AS4/3506-1 laminate as a function of relative delamination area D^{ld}: (a) normalised moduli and Poisson's ratio; (b) shear-extension coupling coefficients. Matrix crack density 2 cracks/cm.

5.3. Strain energy release rate for local delamination

Balanced laminates: As evidenced by Eq. (24), under uniaxial strain SERR varies linearly with the square of the applied strain $\bar{\varepsilon}_{xx}^2$. The normalised SERR $G^{ld}/\bar{\varepsilon}_{xx}^2$ may be used to study the effect of damage separately. Fig. 9 shows the normalised SERR $G^{ld}/\bar{\varepsilon}_{xx}^2$, calculated from Eq. (24) as a function of the delam-

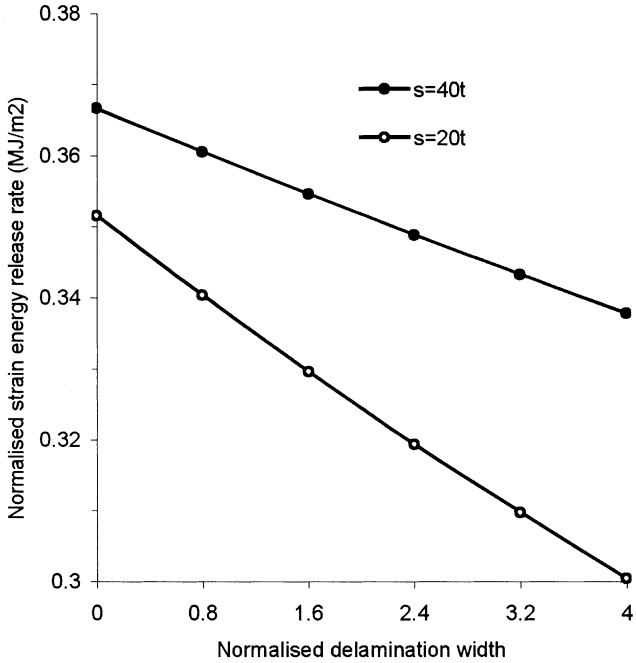

Fig. 9. Normalised SERR $G^{ld}/\bar{\varepsilon}_{xx}^2$ for uniform local delamination in a cracked $[0_2/25_2/-25_2]_s$ AS4/3506-1 laminate as a function of normalised delamination length ℓ/t. Matrix crack spacing $s = 20t$ and 40t.

ination length normalised by the single ply thickness ℓ/t. The laminate lay up is $[0_2/25_2/-25_2]_s$, and crack half spacings are $s = 40t$ and $s = 20t$. This is equivalent to the crack densities of approximately $C = 1$ and 2 cm^{-1} respectively. It can be seen that the present approach gives the SERR for uniform local delamination that depends both on crack density and delamination length. The result of Eq. (25) for the same lay up is found equal to 12.7 MJ/m^2 provided shear-extension coupling and bending-extension coupling are taken into account (O'Brien, 1991). Still, it is much higher than our predictions, since the model of Eq. (25) is for a single isolated matrix crack and associated local delamination and does not account for the cumulative effect of multiple cracking and local delaminations as illustrated in Fig. 2.

Fig. 10 shows predictions of the normalised SERR $G^{ld}/\bar{\varepsilon}_{xx}^2$ associated with uniform local delamination in $[0_2/\theta_2/-\theta_2]_s$ laminates calculated from Eq. (24). Results are plotted as function of the relative delamination area D^{ld} and are given for the range of ply orientation angle θ from 15° to 75°. Matrix crack density in the inner $(-\theta)$ ply of the laminate is assumed equal to $C = 1$ crack/cm. It may be seen that the normalised SERR depends linearly on the relative delamination area, decreasing as the delamination area increases. This relationship is observed for all ply orientation angles up to $D^{ld} = 80\%$, after which the value of $G^{ld}/\bar{\varepsilon}_{xx}^2$ falls more steeply. For the same delamination area, the normalised SERR associated with local delamination is higher for greater values of θ.

Fig. 11 shows predictions of the normalised SERR $G^{ld}/\bar{\varepsilon}_{xx}^2$ at the onset of local delamination ($D^{ld} = 0$) as a function of the crack density in the $(-\theta)$ ply of $[0_2/\theta_2/-\theta_2]_s$ laminates. It can be seen that, for the same crack density, the normalised SERR at the delamination onset is higher for greater values of θ, which will translate into lower onset strain value. For all ply orientation angles θ, SERR at the delamination onset depends linearly on matrix crack density, slightly decreasing as the crack density increases. For instance, for the $[0_2/45_2/-45_2]_s$ laminate the difference between the values of $G^{ld}/\bar{\varepsilon}_{xx}^2$ at 0.5 and 5 cracks/cm is 8.5%.

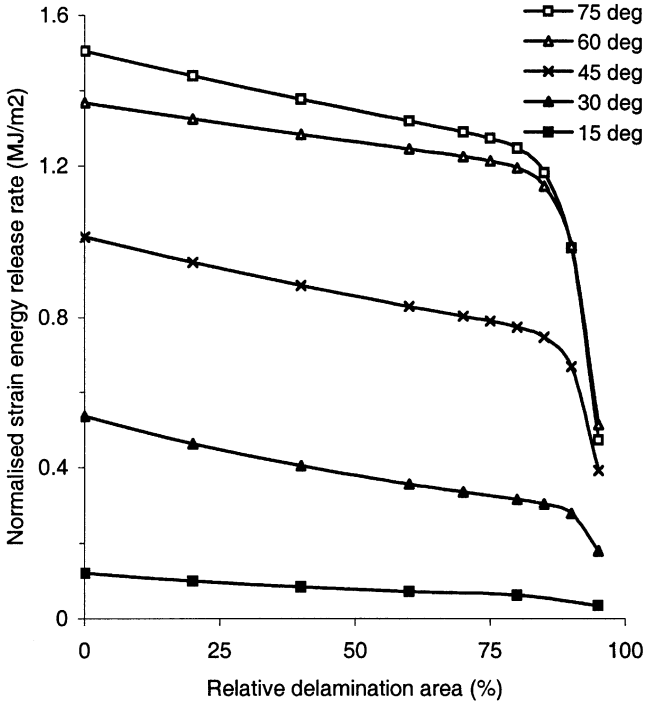

Fig. 10. Normalised SERR $G^{ld}/\bar{\varepsilon}_{xx}^2$ for uniform local delamination in a cracked balanced symmetric $[0_2/\theta_2/-\theta_2]_s$ AS4/3506-1 laminate as a function of relative delamination area D^{ld}. Matrix crack density 1 crack/cm.

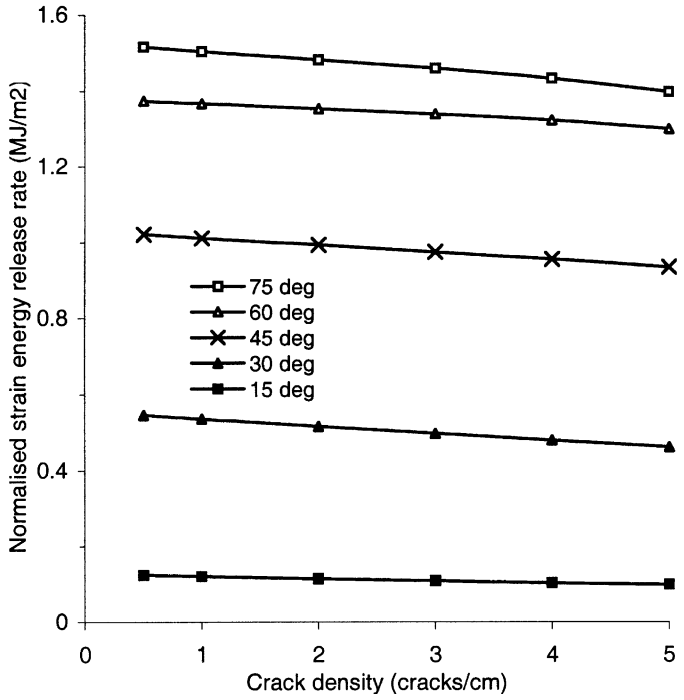

Fig. 11. Normalised SERR $G^{ld}/\bar{\varepsilon}_{xx}^2$ for uniform local delamination in a cracked balanced symmetric $[0_2/\theta_2/-\theta_2]_s$ AS4/3506-1 laminate as a function of crack density. Relative delamination area $D^{ld} = 0$ (onset of delamination).

Reduction in the normalised SERR value will translate into a decrease in the delamination onset strain in laminates with higher matrix crack density.

Using Eqs. (29) and (30), the contributions of mode I and mode II into the total SERR $G^{ld}/\bar{\varepsilon}_{xx}^2$ at the onset of local delamination ($D^{ld} = 0$) are estimated for $[0_2/\theta_2/-\theta_2]_s$ laminates and plotted in Fig. 12 as a function of the cracked $(-\theta)$ ply orientation angle. It can been seen that $G_{\mathrm{I}}^{ld}/\bar{\varepsilon}_{xx}^2$ increases monotonically with increasing θ, while $G_{\mathrm{II}}^{ld}/\bar{\varepsilon}_{xx}^2$ reaches a maximum value at approximately $\theta = 50°$. Also, for $[0_2/30_2/-30_2]_s$ and $[0_2/45_2/-45_2]_s$ laminates $G_{\mathrm{II}}^{ld} > G_{\mathrm{I}}^{ld}$. Fig. 12 suggests that delamination will initiate at relatively low applied strain in a 90° cracked lamina driven mainly by mode I, while in a 15° cracked lamina will initiate at considerably higher applied strain.

Unbalanced laminates: Fig. 13 shows predictions of the normalised SERR $G^{ld}/\bar{\varepsilon}_{xx}^2$ associated with uniform local delamination in unbalanced $[0_2/\theta_2]_s$ laminates calculated from Eq. (24). Results are plotted as a function of the relative delamination area D^{ld} and are given for the range of ply orientation angles θ from 15° to 90°. Matrix crack density in the inner θ ply of the laminate is assumed equal to 1 crack/cm. As in balanced laminates (Fig. 10), SERR decreases as the delamination area increases. However, in unbalanced laminates the dependence of the normalised SERR on the relative delamination area is non-linear for all ply orientation angles. Also, for the same delamination area, the normalised SERR associated with local delamination is not necessarily higher for greater values of θ. For example, for delaminations with $D^{ld} < 40\%$ the value SERR for the $[0/60]_s$ laminate is greater than for the cross-ply $[0/90]_s$ laminate, while for $D^{ld} > 40\%$ the opposite is true.

Fig. 14 shows predictions of the normalised SERR $G^{ld}/\bar{\varepsilon}_{xx}^2$ at the onset of local delamination ($D^{ld} = 0$) as a function of the crack density in the θ ply of $[0_2/\theta_2]_s$ laminates. For all ply orientation angles θ, strain energy-release rate at the delamination onset depends linearly on matrix crack density, slightly decreasing

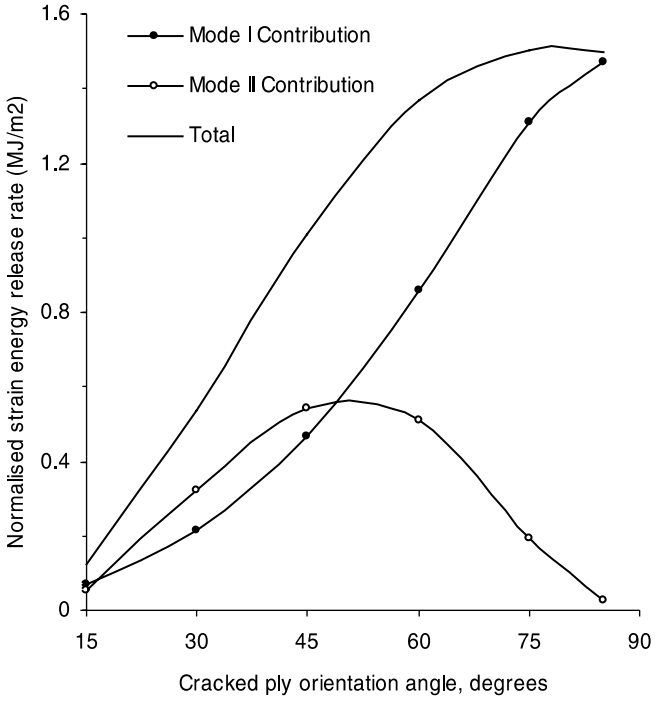

Fig. 12. Normalised SERRs $G_{\mathrm{I}}^{ld}/\bar{\varepsilon}_{xx}^2$ (mode I contribution), $G_{\mathrm{II}}^{ld}/\bar{\varepsilon}_{xx}^2$ (mode II contribution) and $G^{ld}/\bar{\varepsilon}_{xx}^2$ (total) in a cracked balanced symmetric $[0_2/\theta_2/-\theta_2]_s$ AS4/3506-1 laminate as a function of cracked $(-\theta)$ ply orientation angle. Matrix crack density 1 crack/cm, relative delamination area $D^{ld} = 0$ (onset of delamination).

as the crack density increases. This will translate into an increase in the delamination onset strain in laminates with higher matrix crack density.

Contributions of mode I and mode II into the total SERR $G^{ld}/\bar{\varepsilon}_{xx}^2$ at the onset of local delamination $(D^{ld} = 0)$ in $[0_2/\theta_2]_s$ laminates are plotted in Fig. 15 as a function of the cracked θ ply orientation angle. It can been seen that $G_{\mathrm{I}}^{ld}/\bar{\varepsilon}_{xx}^2$ reaches a maximum value at approximately $\theta = 75°$ while $G_{\mathrm{II}}^{ld}/\bar{\varepsilon}_{xx}^2$ reaches a maximum value at approximately $\theta = 55°$.

6. Conclusions

In this paper, local delaminations growing uniformly from the tips of matrix cracks in an angle-ply laminate loaded in tension are modelled theoretically. A 2-D shear-lag analysis is used to determine ply stresses in a representative segment and the equivalent layer model is applied to derive expressions for mode I, mode II and the total SERR associated with uniform local delaminations. These expressions could be used with appropriate fracture criteria to estimate the onset of local delamination in an already cracked off-axis laminate.

Dependence of SERRs and the laminate stiffness properties on delamination area, crack density and ply orientation angle θ is examined for balanced $[0_2/\theta_2/-\theta_2]_s$ and unbalanced $[0_2/\theta_2]_s$ carbon/epoxy laminates. It is found that SERR depends linearly on crack density both in balanced and unbalanced laminates. The dependence on delamination area is linear in balanced and non-linear in unbalanced laminates. Mode I

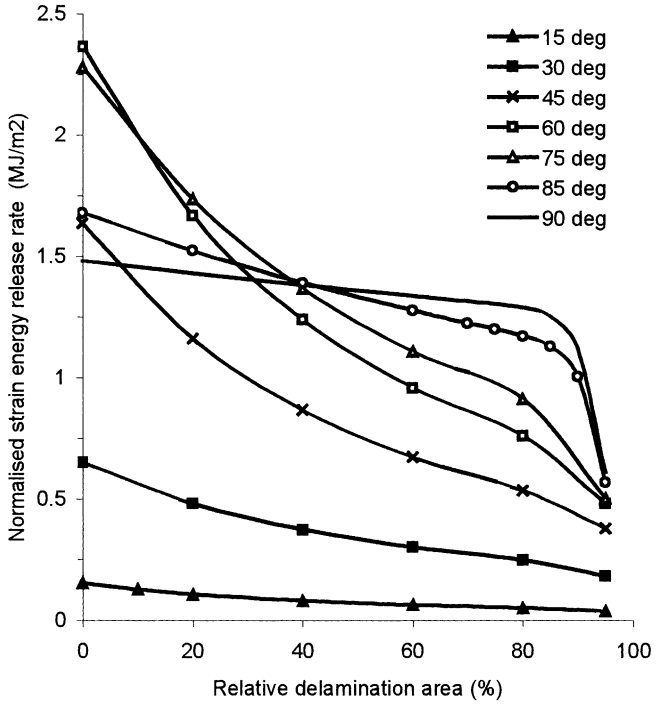

Fig. 13. Normalised SERR $G^{ld}/\bar{\varepsilon}_{xx}^2$ for uniform local delamination in a cracked unbalanced symmetric $[0_2/\theta_2]_s$ AS4/3506-1 laminate as a function of relative delamination area D^{ld}. Crack density 1 crack/cm.

contribution into the total SERR increases monotonically with increasing cracked ply orientation angle in balanced $[0_2/\theta_2/-\theta_2]_s$ laminates and reaches a maximum at $\theta = 75°$ in unbalanced $[0_2/\theta_2]_s$ laminates. However, dependence of mode II contribution on the cracked ply orientation angle in balanced and unbalanced laminates is similar—it reaches a maximum value at θ between 50° and 55°.

Comparison with results obtained by O'Brien (1991) shows that O'Brien's closed-form expression for uniform local delamination significantly overestimates the value of the total SERR leading to lower theoretical strains for the initiation of local delamination and therefore over-conservative designs. Also, it gives the total SERR as independent of delamination area and does not take into account the cumulative effect of damage.

It is established that, for the same ply orientation angle, crack density and delamination area, damage induced changes in stiffness properties are much more significant in unbalanced $[0_2/\theta_2]_s$ laminates than in balanced $[0_2/\theta_2/-\theta_2]_s$ laminates. In near future work, the analytical predictions will be compared to numerical (finite element) and experimental data, which for the lay ups, damage modes and loading conditions examined in this study are currently not available.

Acknowledgements

Financial support of this research by the Engineering and Physical Sciences Research Council (EPSRC/GR/L51348) and the British Ministry of Defence is gratefully acknowledged.

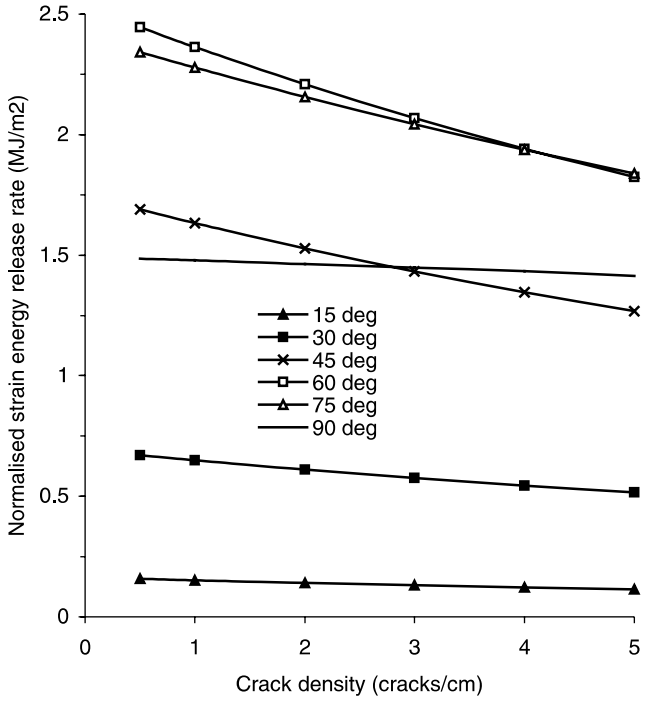

Fig. 14. Normalised SERR $G^{ld}/\bar{\varepsilon}_{xx}^2$ for uniform local delamination in a cracked unbalanced symmetric $[0_2/\theta_2]_s$ AS4/3506-1 laminate as a function of crack density. Relative delamination area $D^{ld} = 0$ (onset of delamination).

Appendix A

Variation of the out-of-plane shear stresses has the form

$$\sigma_{j3}^{(2)} = \frac{\tau_j}{h_2} x_3, \quad 0 \leqslant |x_3| \leqslant h_2, \ \ j = 1,2 \qquad \sigma_{j3}^{(1)} = \frac{\tau_j}{h_1}(h - x_3), \quad h_2 \leqslant |x_3| \leqslant h \tag{A.1}$$

Constitutive equations for the out-of-plane shear stresses

$$\begin{Bmatrix} \sigma_{13}^{(k)} \\ \sigma_{23}^{(k)} \end{Bmatrix} \approx \begin{bmatrix} Q_{55}^{(k)} & Q_{45}^{(k)} \\ Q_{45}^{(k)} & Q_{44}^{(k)} \end{bmatrix} \frac{\partial}{\partial x_3} \begin{Bmatrix} u_1^{(k)} \\ u_2^{(k)} \end{Bmatrix}, \quad i = 1,2 \tag{A.2}$$

After substituting Eq. (A.2) into Eq. (A.1), multiplying them by x_3 and by $h - x_3$ respectively and integrating with respect to x_3 we get

$$\frac{h_1}{3} \begin{Bmatrix} \tau_1 \\ \tau_2 \end{Bmatrix} = \begin{bmatrix} \widehat{Q}_{55}^{(1)} & \widehat{Q}_{45}^{(1)} \\ \widehat{Q}_{45}^{(1)} & \widehat{Q}_{44}^{(1)} \end{bmatrix} \left(\begin{Bmatrix} \tilde{u}_1^{(1)} \\ \tilde{u}_2^{(1)} \end{Bmatrix} - \begin{Bmatrix} V_1 \\ V_2 \end{Bmatrix} \right), \qquad \frac{h_2}{3} \begin{Bmatrix} \tau_1 \\ \tau_2 \end{Bmatrix} = \begin{bmatrix} \widehat{Q}_{55}^{(2)} & \widehat{Q}_{45}^{(2)} \\ \widehat{Q}_{45}^{(2)} & \widehat{Q}_{44}^{(2)} \end{bmatrix} \left(\begin{Bmatrix} V_1 \\ V_2 \end{Bmatrix} - \begin{Bmatrix} \tilde{u}_1^{(2)} \\ \tilde{u}_2^{(2)} \end{Bmatrix} \right) \tag{A.3}$$

Here $\{V\} = \{u^{(1)}\}|_{x_3 = h_2} = \{u^{(2)}\}|_{x_3 = h_2}$ are the in-plane displacements at the interface. After rearranging Eq. (A.3) become

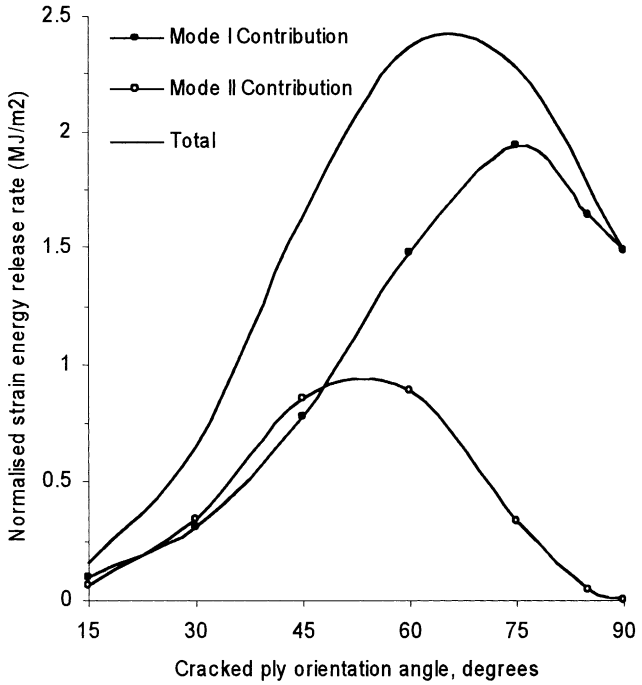

Fig. 15. Normalised SERRs $G_{\mathrm{I}}^{ld}/\bar{\varepsilon}_{xx}^{2}$ (mode I contribution), $G_{\mathrm{II}}^{ld}/\bar{\varepsilon}_{xx}^{2}$ (mode II contribution) and $G^{ld}/\bar{\varepsilon}_{xx}^{2}$ (total) in a cracked unbalanced symmetric $[0_2/\theta_2]_s$ AS4/3506-1 laminate as a function of cracked θ-ply orientation angle. Matrix crack density 1 crack/cm, relative delamination area $D^{ld}=0$ (onset of delamination).

$$\begin{Bmatrix} \tilde{u}_1^{(1)} \\ \tilde{u}_2^{(1)} \end{Bmatrix} - \begin{Bmatrix} \tilde{u}_1^{(2)} \\ \tilde{u}_2^{(2)} \end{Bmatrix} = \left(\frac{h_1}{3} \begin{bmatrix} \widehat{Q}_{55}^{(1)} & \widehat{Q}_{45}^{(1)} \\ \widehat{Q}_{45}^{(1)} & \widehat{Q}_{44}^{(1)} \end{bmatrix}^{-1} + \frac{h_2}{3} \begin{bmatrix} \widehat{Q}_{55}^{(2)} & \widehat{Q}_{45}^{(2)} \\ \widehat{Q}_{45}^{(2)} & \widehat{Q}_{44}^{(2)} \end{bmatrix}^{-1} \right) \begin{Bmatrix} \tau_1 \\ \tau_2 \end{Bmatrix} \tag{A.4}$$

Inversion of Eq. (A.4) leads to

$$\begin{Bmatrix} \tau_1 \\ \tau_2 \end{Bmatrix} = \begin{bmatrix} K_{11} & K_{12} \\ K_{21} & K_{22} \end{bmatrix} \left(\begin{Bmatrix} \tilde{u}_1^{(1)} \\ \tilde{u}_2^{(1)} \end{Bmatrix} - \begin{Bmatrix} \tilde{u}_1^{(2)} \\ \tilde{u}_2^{(2)} \end{Bmatrix} \right) \tag{A.5}$$

with

$$[K] = \left(\frac{h_1}{3} \begin{bmatrix} \widehat{Q}_{55}^{(1)} & \widehat{Q}_{45}^{(1)} \\ \widehat{Q}_{45}^{(1)} & \widehat{Q}_{44}^{(1)} \end{bmatrix}^{-1} + \frac{h_2}{3} \begin{bmatrix} \widehat{Q}_{55}^{(2)} & \widehat{Q}_{45}^{(2)} \\ \widehat{Q}_{45}^{(2)} & \widehat{Q}_{44}^{(2)} \end{bmatrix}^{-1} \right)^{-1} \tag{A.6}$$

Appendix B

On referring to the constitutive equations, Eqs. (6a) and (6b), the generalised plane strain condition, Eq. (5), becomes

$$\widehat{S}_{11}^{(1)}\tilde{\sigma}_{11}^{(1)} + \widehat{S}_{12}^{(1)}\tilde{\sigma}_{22}^{(1)} + \widehat{S}_{16}^{(1)}\tilde{\sigma}_{12}^{(1)} = \widehat{S}_{11}^{(2)}\tilde{\sigma}_{11}^{(2)} + \widehat{S}_{12}^{(2)}\tilde{\sigma}_{22}^{(2)} \tag{B.1}$$

Using the laminate equilibrium equations, Eqs. (4a)–(4c), stresses in the constraining layer (layer 1) can be excluded, so that the microstress component $\tilde{\sigma}_{11}^{(2)}$ is given by

$$\tilde{\sigma}_{11}^{(2)} = a_{22}\tilde{\sigma}_{22}^{(2)} + a_{12}\tilde{\sigma}_{12}^{(2)} + b_x\bar{\sigma}_x + b_y\bar{\sigma}_y \tag{B.2}$$

$$a_{22} = -\frac{\widehat{S}_{12}^{(1)} + \chi\widehat{S}_{12}^{(2)}}{\widehat{S}_{11}^{(1)} + \chi\widehat{S}_{11}^{(2)}}, \qquad a_{12} = -\frac{\widehat{S}_{16}^{(1)}}{\widehat{S}_{11}^{(1)} + \chi\widehat{S}_{11}^{(2)}}$$

$$b_x = \frac{(1+\chi)(\widehat{S}_{11}^{(1)}\cos^2\phi + \widehat{S}_{12}^{(1)}\sin^2\phi - \widehat{S}_{16}^{(1)}\sin\phi\cos\phi)}{\widehat{S}_{11}^{(1)} + \chi\widehat{S}_{11}^{(2)}}$$

$$b_y = \frac{(1+\chi)(\widehat{S}_{11}^{(1)}\sin^2\phi + \widehat{S}_{12}^{(1)}\cos^2\phi + \widehat{S}_{16}^{(1)}\sin\phi\cos\phi)}{\widehat{S}_{11}^{(1)} + \chi\widehat{S}_{11}^{(2)}}$$

Strain differences are expressed in terms of stresses as

$$\begin{Bmatrix} \tilde{\gamma}_{12}^{(1)} - \tilde{\gamma}_{12}^{(2)} \\ \tilde{\varepsilon}_{22}^{(1)} - \tilde{\varepsilon}_{22}^{(2)} \end{Bmatrix} = -\frac{1}{\chi}\begin{bmatrix} L_{11} & L_{12} \\ L_{21} & L_{22} \end{bmatrix}\begin{Bmatrix} \tilde{\sigma}_{12}^{(2)} \\ \tilde{\sigma}_{22}^{(2)} \end{Bmatrix} + \frac{1}{\chi}\begin{bmatrix} M_{11} & M_{12} \\ M_{21} & M_{22} \end{bmatrix}\begin{Bmatrix} \bar{\sigma}_x \\ \bar{\sigma}_y \end{Bmatrix} \tag{B.3}$$

Here

$$L_{11} = \widehat{S}_{66}^{(1)} + a_{12}\widehat{S}_{16}^{(1)} + \chi\widehat{S}_{66}^{(2)}, \qquad L_{12} = \widehat{S}_{26}^{(1)} + a_{22}\widehat{S}_{16}^{(1)}$$

$$L_{21} = \widehat{S}_{26}^{(1)} + a_{12}\widehat{S}_{12}^{(1)} + \chi a_{12}\widehat{S}_{12}^{(2)}, \qquad L_{22} = \widehat{S}_{22}^{(1)} + a_{22}\widehat{S}_{12}^{(1)} + \chi(\widehat{S}_{22}^{(2)} + a_{22}\widehat{S}_{12}^{(2)}) \tag{B.4a}$$

$$\begin{aligned}
M_{11} &= (1+\chi)\left[(\widehat{S}_{16}^{(1)} + a_{12}\widehat{S}_{11}^{(2)})\cos^2\phi + (\widehat{S}_{26}^{(1)} + a_{12}\widehat{S}_{12}^{(1)})\sin^2\phi - (\widehat{S}_{66}^{(1)} + a_{12}\widehat{S}_{16}^{(1)})\sin\phi\cos\phi\right] \\
M_{21} &= (1+\chi)\left[(\widehat{S}_{12}^{(1)} + a_{22}\widehat{S}_{11}^{(1)})\cos^2\phi + (\widehat{S}_{22}^{(1)} + a_{22}\widehat{S}_{12}^{(1)})\sin^2\phi - (\widehat{S}_{26}^{(1)} + a_{22}\widehat{S}_{16}^{(1)})\sin\phi\cos\phi\right] \\
M_{12} &= (1+\chi)\left[(\widehat{S}_{16}^{(1)} + a_{12}\widehat{S}_{11}^{(2)})\sin^2\phi + (\widehat{S}_{26}^{(1)} + a_{12}\widehat{S}_{12}^{(1)})\cos^2\phi + (\widehat{S}_{66}^{(1)} + a_{12}\widehat{S}_{16}^{(1)})\sin\phi\cos\phi\right] \\
M_{22} &= (1+\chi)\left[(\widehat{S}_{12}^{(1)} + a_{22}\widehat{S}_{11}^{(1)})\sin^2\phi + (\widehat{S}_{22}^{(1)} + a_{22}\widehat{S}_{12}^{(1)})\cos^2\phi + (\widehat{S}_{26}^{(1)} + a_{22}\widehat{S}_{16}^{(1)})\sin\phi\cos\phi\right]
\end{aligned} \tag{B.4b}$$

Substitution into the equilibrium equations (Eq. (3)) yields the following coupled 2nd order differential equations

$$\frac{\mathrm{d}^2}{\mathrm{d}x_2}\begin{Bmatrix} \tilde{\sigma}_{12}^{(2)} \\ \tilde{\sigma}_{22}^{(2)} \end{Bmatrix} - \frac{1}{h_1}\begin{bmatrix} K_{11} & K_{12} \\ K_{21} & K_{22} \end{bmatrix}\left(\begin{bmatrix} L_{11} & L_{12} \\ L_{21} & L_{22} \end{bmatrix}\begin{Bmatrix} \tilde{\sigma}_{12}^{(2)} \\ \tilde{\sigma}_{22}^{(2)} \end{Bmatrix} + \begin{bmatrix} M_{11} & M_{12} \\ M_{21} & M_{22} \end{bmatrix}\begin{Bmatrix} \bar{\sigma}_x \\ \bar{\sigma}_y \end{Bmatrix}\right) = 0 \tag{B.5}$$

or

$$\frac{\mathrm{d}^2}{\mathrm{d}x_2}\begin{Bmatrix} \tilde{\sigma}_{12}^{(2)} \\ \tilde{\sigma}_{22}^{(2)} \end{Bmatrix} - \begin{bmatrix} N_{11} & N_{12} \\ N_{21} & N_{22} \end{bmatrix}\begin{Bmatrix} \tilde{\sigma}_{12}^{(2)} \\ \tilde{\sigma}_{22}^{(2)} \end{Bmatrix} + \begin{bmatrix} P_{11} & P_{12} \\ P_{21} & P_{22} \end{bmatrix}\begin{Bmatrix} \bar{\sigma}_x \\ \bar{\sigma}_y \end{Bmatrix} = 0 \tag{B.6}$$

where $[N] = h_1^{-1}[K][L]$ and $[P] = h_1^{-1}[K][M]$, with matrices $[K]$, $[L]$ and $[M]$ defined by Eqs. (A.6), (B.4a) and (B.4b) respectively.

Appendix C

$$A_1 = \frac{\lambda_1^2 - N_{22}}{N_{21}} A_2, \qquad B_1 = \frac{\lambda_2^2 - N_{22}}{N_{21}} B_2, \qquad C_1 = -\frac{C_2 N_{22} + P_{21} + \alpha P_{22}}{N_{21}} \tag{C.1}$$

$$A_2 = -\frac{(P_{21} + \alpha P_{22})(N_{21}N_{12} - N_{11}N_{22}) + R\lambda_2^2}{(\lambda_2^2 - \lambda_1^2)(N_{21}N_{12} - N_{11}N_{22})}, \qquad B_2 = \frac{(P_{21} + \alpha P_{22})(N_{21}N_{12} - N_{11}N_{22}) + R\lambda_1^2}{(\lambda_2^2 - \lambda_1^2)(N_{21}N_{12} - N_{11}N_{22})} \tag{C.2}$$

$$C_2 = \frac{R}{N_{21}N_{12} - N_{11}N_{22}}, \qquad R = N_{11}(P_{21} + \alpha P_{22}) - N_{21}(P_{11} + \alpha P_{12}) \tag{C.3}$$

References

Armanios, E.A., Sriram, P., Badir, A.M., 1991. Fracture analysis of transverse crack-tip and free-edge delamination in laminated composites. In: O'Brien, T.K. (Ed.), Composite Materials: Fatigue and Fracture, ASTM STP 1110. ASTM, Philadelphia, PA.

Ashkantala, N., Talreja, R., 1998. A mechanistic model for fatigue damage evolution for composite laminates. Mechanics of Materials 29 (2), 123–140.

Berthelot, J.M., Le Corre, J.F., 2000. A model for transverse cracking and delamination in cross-ply laminates. Composites Science and Technology 60 (7), 1055–1066.

Bystrov, V.M., 2000. Analysis of the decay of edge effects in laminated materials on the basis of a representative element. International Applied Mechanics 36 (6), 826–834.

Crossman, F.W., Wang, A.S.D., 1982. The dependence of transverse cracking and delamination on ply thickness in graphite epoxy laminates. In: Riefsnider, K.L. (Ed.), Damage in Composite Materials, ASTM STP 775. ASTM, Philadelphia, PA.

Daniel, I.M., Ishai, O., 1994. Engineering Mechanics of Composite Materials. Oxford University Press, New York.

Dharani, L.R., Tang, H., 1990. Micromechanics characterization of sublaminate damage. International Journal of Fracture 46 (2), 123–140.

Fan, J., Zhang, J., 1993. In-situ damage evolution and micro/macro transition for laminated composites. Composites Science and Technology 47 (2), 107–118.

Kashtalyan, M., Soutis, C., 1999. A study of matrix crack tip delaminations and their influence on composite laminate stiffness. Advanced Composites Letters 8 (4), 149–156.

Kashtalyan, M., Soutis, C., 2000a. The effect of delaminations induced by transverse cracking and splitting on stiffness properties of composite laminates. Composites Part A: Applied Science and Manufacturing 31 (2), 107–119.

Kashtalyan, M., Soutis, C., 2000b. Modelling stiffness degradation due to matrix cracking in angle-ply composite laminates. Plastics, Rubber and Composites 29 (9), 482–488.

Nairn, J.A., Hu, S., 1992. The initiation and growth of delaminations induced by matrix microcracks in laminated composites. International Journal of Fracture 57 (1), 1–24.

O'Brien, T.K., 1982. Characterization of delamination onset and growth in a composite laminate. In: Reifsnider, K.L. (Ed.), Damage in Composite Materials, ASTM STP 775. ASTM, Philadelphia, PA.

O'Brien, T.K., 1985. Analysis of local delamination and their influence on composite laminate behavior. In: Johnson, W.S. (Ed.), Delamination and Debonding of Materials, ASTM STP 876. ASTM, Philadephia, PA.

O'Brien, T.K., 1991. Local delamination in laminates with angle ply matrix cracks: Part II Delamination fracture analysis and fatigue characterization. NASA Technical Memorandum 104076/AVSCOM Technical Report 91-B-011.

O'Brien, T.K., Hooper, S.J., 1991. Local delamination in laminates with angle ply matrix cracks: Part I Tension tests and stress analysis. NASA Technical Memorandum 104055/AVSCOM Technical Report 91-B-010.

Ogihara, S., Takeda, N., 1995. Interaction between transverse cracks and delamination during damage progress in CFRP cross-ply laminates. Composites Science and Technology 54 (4), 395–404.

Salpekar, S.A., O'Brien, T.K., 1991. Combined effect of matrix cracking and free edge on delamination. In: O'Brien, T.K. (Ed.), Composite Materials: Fatigue and Fracture, ASTM STP 1110. ASTM, Philadelphia, PA.

Salpekar, S.A., O'Brien, T.K., 1993. Analysis of matrix cracking and local delamination in $(0/\theta/-\theta)_s$ graphite epoxy laminates under tensile load. ASTM Journal of Composites Technology and Research 15 (2), 95–100.

Salpekar, S.A., O'Brien, T.K., Shivakumar, K.N., 1996. Analysis of local delaminations caused by angle-ply matrix cracks. Journal of Composite Materials 30 (4), 418–440.

Selvarathinam, A.S., Weitsman, Y.J., 1998. Transverse cracking and delamination in cross-ply gr/ep composites under dry, saturated and immersed fatigue. International Journal of Fracture 91 (2), 103–116.

Selvarathinam, A.S., Weitsman, Y.J., 1999. A shear-lag analysis of transverse cracking and delamination in cross-ply carbon-fibre/epoxy composites under dry, saturated and immersed fatigue conditions. Composites Science and Technology 59 (14), 2115–2123.

Soutis, C., Kashtalyan, M., 2000. Delamination growth and residual properties of cracked orthotropic laminates under tensile loading. In: Ochoa, O.O., O'Brien, T.K., Lagoudas D., Sue, H.J. (Eds.), Proceedings of the 15th Annual Technical Conference of ASC/ASTM, 25–27 September 2000, Texas A&M University, TX, USA. pp. 1153–1160.

Takeda, N., Ogihara, S., 1994. Initiation and growth of delamination from the tip of transverse cracks in CFRP cross-ply laminates. Composites Science and Technology 52 (3), 309–318.

Zhang, J., Fan, J., Herrmann, K.P., 1999. Delaminations induced by constrained transverse cracking in symmetric composite laminates. International Journal of Solids and Structures 36 (6), 813–846.

Zhang, J., Soutis, C., Fan, J., 1994a. Effects of matrix cracking and hygrothermal stresses on the strain energy release rate for edge delamination in composite laminates. Composites 25 (1), 27–35.

Zhang, J., Soutis, C., Fan, J., 1994b. Strain energy release rate associated with local delamination in cracked composite laminates. Composites 25 (9), 851–862.